Translational Stroke Research
https://doi.org/10.1007/s12975-025-01384-8

RESEARCH

Identification of Biomarkers Related to the Pathogenesis and Prognosis of Pediatric Moyamoya Disease Via Cerebrospinal Fluid Proteomics

Youngbo Shim[1,2] · Seung Ah Choi[1,3,4] · Kisoon Dan[5] · Eun Jung Koh[1,3] · Saehim Ha[1,3] · Ji Hoon Phi[1,3,4] · Joo Whan Kim[1,3,6] · Dohyun Han[5,7] · Seung-Ki Kim[1,3,4]

Received: 16 May 2025 / Revised: 5 September 2025 / Accepted: 16 September 2025

Abstract

Developing cost-effective, noninvasive biomarker-based tests could transform moyamoya disease (MMD) management. This study aimed to identify clinically relevant cerebrospinal fluid (CSF) biomarkers through comprehensive proteomic screening in a large MMD cohort. CSF protein profiles from 104 MMD patients and 14 non-tumorous hydrocephalus patients were analyzed via liquid chromatography-tandem mass spectrometry. Enrichment analysis was conducted on canonical pathways and differentially expressed proteins (DEPs). The protein–protein interaction network data included all proteins involved in canonical pathways. Potential markers were validated via ELISA. Weighted gene coexpression network analysis (WGCNA) revealed clinical factor-related modules. We identified 2463 proteins, and 2307 were quantified in at least one sample. A total of 321 significant DEPs were identified, with 8 proteins upregulated and 11 proteins downregulated in MMD samples. ELISA confirmed the increased expression of ALB and SLITRK1. WGCNA revealed seven modules correlated with clinical factors, linking preoperative cerebral infarction to the module eigengene (ME) red module and favorable modified Rankin scale scores to the MEblack module. BASP1 and LDHA were significantly upregulated in MEred, whereas CD9 and EMILIN1 were upregulated in MEblack. Our findings shed light on the proteomics of CSF from MMD patients, identifying potential novel biomarkers such as SLITRK1 and markers of preoperative cerebral infarction (BASP1, LDHA) and clinical outcome (CD9, EMILIN1). These markers have potential as new diagnostic and therapeutic targets for MMD.

Keywords Moyamoya disease · Proteomics · Cerebrospinal fluid · Biomarkers

Abbreviations

MMD	Moyamoya disease
ICA	Internal carotid artery
RNF	Ring finger protein
CSF	Cerebrospinal fluid

Communicated by Huimahn Choi.

Youngbo Shim, Seung Ah Choi, and Kisoon Dan contributed equally to this work.

✉ Dohyun Han
hdh03@snu.ac.kr

✉ Seung-Ki Kim
nsthomas@snu.ac.kr

[1] Division of Pediatric Neurosurgery, Pediatric Clinical Neuroscience Center, Seoul National University Children's Hospital, Seoul, Republic of Korea

[2] Department of Critical Care Medicine, Kangbuk Samsung Hospital, Sungkyunkwan University School of Medicine, Seoul, Republic of Korea

[3] Department of Neurosurgery, Seoul National University Hospital, Seoul National University College of Medicine, Seoul, Republic of Korea

[4] Neuroscience Research Institute, Seoul National University College of Medicine, Seoul, Republic of Korea

[5] Proteomics Core Facility, Biomedical Research Institute, Seoul National University Hospital, Seoul, Republic of Korea

[6] Department of Genomic Medicine, Seoul National University Hospital, Seoul, Republic of Korea

[7] Department of Transdisciplinary Medicine, Seoul National University Hospital, Seoul, Republic of Korea

Published online: 01 October 2025

CNS	Central nervous system
CRABP	Cellular retinoic acid-binding protein
LC–MS/MS	Liquid chromatography with tandem mass spectrometry
HC	Hydrocephalus
ELISA	Enzyme-linked immunosorbent assay
OD	Optical density
iBAQ	Intensity-based absolute quantification
DEP	Differentially expressed protein
IPA	Ingenuity pathway analysis
PPI	Protein−protein interaction
WGCNA	Weighted gene coexpression network analysis
PCA	Principal component analysis
ECM	Extracellular matrix
FCBF	Fast correlation-based filter
AUROC	Area under the receiver-operating characteristics curve
ME	Module eigengene
GO	Gene Ontology

Introduction

Moyamoya disease (MMD) is characterized by progressive stenosis or occlusion of distal internal carotid arteries (ICAs) and their major branches [1, 2]. Histologically, MMD patients exhibit fibrocellular thickening of the tunica intima, irregular undulation of the internal elastic lamina, and attenuation of the tunica media [3]. This leads to hypoperfusion, the formation of multiple collateral vessels, and distinctive "puffs of smoke" angiographic findings. Ischemic strokes result from hypoperfusion, whereas hemorrhagic strokes stem from collateral vessel rupture [4]. MMD manifests differently by age, with children experiencing mainly ischemic symptoms and adults often suffering from intracranial hemorrhage (ICH). Progression is faster in children, with one-third worsening without surgery [5] and 20% developing severe disabilities [6]. Current treatments involve revascularization surgery, such as encephalo-duro-arteriosynangiosis or superficial temporal artery−middle cerebral artery anastomosis [7], to stabilize blood flow and regress collateral vessels [8].

Most patients are diagnosed after disease progression, and some patient groups, particularly young children under 3 years of age, may experience a rapid and fulminant decline [9]. Moreover, certain patients fail to develop adequate collateral circulation even after surgical revascularization [7]. Owing to its unclear pathogenesis, developing pharmacological therapies to prevent or halt disease progression is challenging. A deeper understanding of MMD pathogenesis is essential for establishing medical treatments that can prevent or slow its progression.

Currently, the gold standard for diagnosing MMD is digital subtraction angiography, which is invasive and often requires sedation or anesthesia in children due to poor cooperation. The development of cost-effective, noninvasive biomarker-based screening tests may revolutionize the management of MMD, particularly in pediatric patients. Studies on various biomarkers in blood have been conducted, including genetic markers such as Ring finger protein 213 (RNF 213) [10, 11], ZXD family zinc finger, and obscurin [12], as well as molecular biomarkers such as vascular smooth muscle enzymes and growth factors [13]. However, none have demonstrated clinical utility for diagnosis, treatment, or prognostic evaluation.

Cerebrospinal fluid (CSF) represents a valuable source for identifying biomarkers of neurological diseases affecting the central nervous system (CNS), and multiple efforts have been made to explore its potential. Although candidate therapeutic targets such as cellular retinoic acid-binding protein (CRABP)−1 [14], gamma-carboxylation of the Glu-42 transthyretin [15], a 4473 Da peptide [16], and alterations in haptoglobin and apolipoproteins [17] have been reported, these findings are based on small patient cohorts ($N = 10$ to 29) and their clinical utility remains unproven.

In this study, we performed comprehensive proteomic screening of CSF using liquid chromatography with tandem mass spectrometry (LC–MS/MS) in an expanded cohort of MMD patients to identify novel biomarkers and evaluate their clinical significance.

Experimental Procedures

Patients Sample Collection

Peripheral blood and CSF samples were obtained from 104 MMD patients and 14 non-tumorous hydrocephalus (HC) patients. Clinical data were collected for all patients. MMD was diagnosed by cerebral angiography, with bilaterality (definite: bilateral; probable: unilateral) and preoperative angiographic findings assessed according to the Suzuki staging system [2]. Preoperative cerebral infarction and ICH were evaluated via magnetic resonance imaging, and surgical laterality (bilateral or unilateral) was documented. The modified Rankin scale (mRS) score was assessed at the last follow-up, with scores ranging from 0 to 6; scores of 0 to 2 were defined as favorable clinical outcomes, whereas scores ≥ 3 were considered unfavorable. An mRS of 3 represents moderate disability, indicating loss of independent living ability [18].

Peripheral blood samples from MMD patients were obtained via radial artery catheterization during indirect bypass surgery under general anesthesia. Blood was collected in EDTA tubes, and plasma was separated by

centrifugation. Genomic DNA was then extracted from 200 µL of whole blood using the MasterPure™ Complete DNA Purification Kit (Biosearch Technologies, Middleton, WI).

To detect the RNF213 c.14429G>A (p.R4810K) variant, targeted sequencing was performed. Genomic DNA was extracted from patient blood samples, and the target region was amplified using BioFACT 2xLamp Taq PCR Master Mix (BIOFACTORY, Daejeon, Korea) on a BioFACT Hush Run™ PCR Machine with primers AGA_F (5′-CTG ATG CGT CAG CTC CAT-3′) and AGA_R (5′-TTC CTG CTT TGT GCA GTC-3′). The PCR products were sequenced via the ABI BigDye Terminator v3.1 Cycle Sequencing Kit (Thermo Fisher Scientific, Waltham, MA, USA). Genotypes at the c.14429G>A locus were categorized as homozygous wild type (G/G), heterozygous (G/A), or homozygous mutant (A/A). Demographic and clinical characteristics according to genotype were compared using the Mann–Whitney *U* test, Fisher's exact test, and the Cochran–Armitage trend test. All statistical analyses were conducted with R software (version 4.4.1; R Foundation for Statistical Computing, Vienna, Austria), with statistical significance set at $P < 0.05$ and a 95% confidence interval.

CSF analysis was limited to patients from whom samples were collected prior to the first surgery. In MMD patients, approximately 10 mL of CSF was obtained by aspiration through a small incision in the arachnoid membrane immediately after dural opening, using a 2.5-mL syringe. In HC patients, CSF was collected from the ventricle during endoscopic third ventriculostomy or shunting procedures. All samples were confirmed to be free of blood contamination.

This study was approved by the Institutional Review Board of our institution (No. 2011-191-1178), and informed consent was waived due to its retrospective study design. The study was conducted in accordance with the principles of the Declaration of Helsinki. The mass spectrometry proteomics data have been deposited in the ProteomeXchange Consortium via the PRIDE [19] partner repository with the dataset identifier PXD059285.

Preparation of CSF Samples for Proteomics

For protein digestion, 100–200 µL of each CSF sample was dried via speed-vac and reconstituted in 50 µL of SDT buffer (2% SDS, 0.1 M dithiothreitol [DTT] in 0.1 M Tris–HCl, pH 8.0). After being heated at 95 ℃, the denatured proteins were digested via a filter-aided sample preparation (FASP) method as previously described [20] with some modifications. Briefly, protein samples were loaded onto a 30 K Amicon filter (Millipore, Billerica, MA, USA), and the buffer was exchanged with UA solution (8 M urea in 0.1 M Tris–HCl, pH 8.5) via centrifugation. Following three buffer exchanges with UA solution, reduced cysteines were alkylated with 0.05 M iodoacetamide (IAA) in UA solution for 30 min at room temperature in the dark.

Subsequently, the UA buffer was exchanged twice with 40 mM ammonium bicarbonate (ABC). Proteins were digested with trypsin/LysC (enzyme to substrate ratio of 1:100) at 37 ℃ for 16 h. The resulting peptides were collected in new Eppendorf tubes via centrifugation, and an additional elution step was performed using 40 mM ABC and 0.5 M NaCl. After acidification with 10% trifluoroacetic acid, the peptides were desalted and fractionated on homemade styrene-divinylbenzene reversed-phase sulfonate (SDB) stage tips in basic reversed-phase via a stepwise gradient of acetonitrile (40%, 60%, and 80%) in 1% ammonium hydroxide as described previously [20]. The fractionated peptides were dried completely in a vacuum dryer and stored at −80 °C.

Establishment of a Matching Spectral Library

To construct a spectral library for matching between runs [21, 22], a MARS-14 column (Agilent Technologies, Santa Clara, CA, USA) was employed to deplete the 14 highest–abundance proteins following the manufacturer's instructions. The depleted samples were digested via the two-step FASP method as previously described [20], and the resulting peptides were desalted via custom C18 StageTips. For the in-depth dataset, 25 µg of purified peptides were fractionated on an Agilent 1260 Bio-inert HPLC system (Agilent Technologies) equipped with an analytical column (4.6 × 250 mm, 5-µm particle). High-pH reversed-phase peptide fractionation was carried out at a flow rate of 0.8 mL/min over a 60 min gradient using solvent A (15 mM ammonium hydroxide in water) and solvent B (15 mM ammonium hydroxide in 90% acetonitrile). Ninety-six fractions were collected each minute and noncontiguously pooled into 24 fractions. The fractions were dried in a vacuum centrifuge and stored at −80 °C until LC–MS/MS analysis.

LC–MS/MS Analysis

LC–MS/MS analysis was conducted via Quadrupole Orbitrap mass spectrometers, Q Exactive HF-X (Thermo Fisher Scientific, Waltham, MA, USA) coupled to an Ultimate 3000 RSLC system (Dionex, Sunnyvale, CA, USA) with a nano-electrospray source, following a previously described protocol with some modifications [23]. Peptides were separated via a two-column configuration consisting of a trap column (500 µm I.D. × 0.5 mm, C18, 5 µm) and an analytical column (75 µm I.D. × 50 cm, C18 1.9 µm, 100 Å). Dried peptide samples were reconstituted in solvent A (2% acetonitrile, 0.1% formic acid) prior to injection. Upon loading onto the nano-LC system, a 90-min gradient from 8 to 30% solvent B (100% acetonitrile and 0.1% formic acid) was applied

to all the samples. The spray voltage was set to 2.0 kV in positive ion mode, and the heated capillary temperature was maintained at 320 °C. Mass spectra were acquired in data-dependent mode via the top 15 method on the Q Exactive. The Orbitrap analyzer scanned precursor ions within a mass range of 300–1650 m/z at a resolution of 70,000 at m/z 200. Higher-energy collisional dissociation (HCD) scans were acquired on the Q Exactive at a resolution of 17,500 with a normalized collision energy of 28. Maximum ion injection times were set to 20 ms for the survey and 120 ms for MS/MS scans.

Database Search

The mass spectra were analyzed via MaxQuant (Version 1.6.1.0) [21]. MS/MS spectra were searched against the Human UniProt protein sequence database (December 2014, 88,657 entries) via the Andromeda search engine [24]. The precursor ion mass tolerance was set to 6 ppm, and fragment ion tolerance was set to 20 ppm. Cysteine carbamido-methylation was specified as a fixed modification, while N-acetylation of proteins and oxidation of methionine were set as variable modifications. Enzyme specificity was defined as full tryptic digestion, considering peptides with a minimum length of six amino acids and allowing up to two missed cleavages. The false discovery rate (FDR) threshold was controlled at 1% at the peptide, protein, and modification levels. To maximize the number of quantification events across samples, matching between runs was conducted utilizing the depleted sample as a spectral library.

Enzyme-Linked Immunosorbent Assay (ELISA) of CSF Samples

The concentrations of ALB, BLVRA, F13A1, VIM, CNDP1, SLITRK1, OGN, and PKM in CSF samples were quantified using ELISA kits, following the manufacturer's instructions. For validation, a total of 40 CSF samples were analyzed, including 34 from MMD patients and 6 from HC patients. Among these, an independent validation set that did not overlap with the discovery proteomics cohort consisted of 13 MMD and 4 HC samples. The concentrations of the proteins in the samples were determined by assessing the absorbance values (optical density, OD) against the standard curve generated during each ELISA. This facilitated the calculation of concentrations for unknown samples. All measurements were performed in triplicate to ensure the reproducibility and reliability.

Experimental Design and Statistical Rationale

Data preprocessing was performed via Perseus software [25]. Proteins identified solely as site-specific, reverse, or contaminants were excluded. Expression levels in CSF were quantified using intensity-based absolute quantification (iBAQ) values computed by MaxQuant. To correct for the skewed distribution, iBAQ values were $\log_2$-transformed. Valid values were filtered to retain proteins with a minimum of 70% quantified values in at least one diagnostic group. Missing values were imputed from a normal distribution (width = 0.5, downshift = 1.8) to simulate signals of low-abundance proteins. Quantile normalization was then applied across all samples to minimize systematic variations. Two-sided *t*-tests were conducted to compare MMD and HC groups, and differentially expressed proteins (DEPs) were identified using an FDR threshold of 5%. For hierarchical clustering, protein abundances were z-normalized, and a heatmap was generated with Pearson's correlation distance as a measure of similarity.

Canonical pathways were analyzed via ingenuity pathway analysis (IPA; QIAGEN, Hilden, Germany) [26] based on DEPs with matched gene names. The analytical algorithms integrated in IPA utilize lists of DEPs to predict biological processes and canonical pathways. Pathways with a Fisher's exact $P < 0.05$ and a $|z| > 0$ were considered significant. Protein–protein interaction (PPI) network data were obtained from the STRING database [27], encompassing all proteins involved in activated or inhibited canonical pathways in MMD.

Weighted gene coexpression network analysis (WGCNA, Version 1.71) was performed on 104 MMD datasets via the R package [28]. Prior to WGCNA, sample clustering with the hclust function identified potential outliers. Protein network construction used a soft-thresholding power β of 12. Modules were defined using the following parameters: minModuleSize of 30, deepSplit of 4, cutHeight of 0.25, threshold percentage of 50, and merge percentage of 25. Functional enrichment analysis was performed for proteins in each module, and PPI analysis was carried out using the STRING database (Version 11.5) [29, 30]. Coexpression networks were visualized with Cytoscape (Version 3.9.1) [31].

Cell-type enrichment analysis was performed using the Brain Expression Spatiotemporal Pattern (BEST) tool [32]. Cell type-specific expression profiles, which provide specific expression gene sets for astrocytes, endothelial cells, microglia, neurons, and oligodendrocytes, were obtained from http://www.brainrnaseq.org [33]. Fisher's exact tests were conducted between each protein and cell type, with the negative logarithm of the *P* value representing the enrichment score.

Results

Patient Characteristics

The sex ratio did not differ significantly between the 104 MMD and 14 HC patients (MMD: male 53% vs. HC: male

50%). However, HC patients were significantly younger (2.5 ± 4.1 years) than MMD patients (8.1 ± 4.1 years, Table 1). Among MMD patients (Table 2), 86% (*N* = 89) had definite MMD, with Suzuki stage 2 being the most frequent (*N* = 47, 45%), followed by Grades 3, 4, 1, and 5 in decreasing order. When Suzuki stages were dichotomized, early stages were more prevalent (Grades 1–3: *N* = 78 vs. Grades 4–6: *N* = 26). Preoperative cerebral infarction was present in 28% (*N* = 29), and preoperative ICH occurred in 3% (*N* = 3). Surgery was performed bilaterally in 79% (*N* = 82). According to the RNF 213 p.R4810K genotype, previously reported to be associated with clinical course and disease severity [34–36], patients were classified into three groups: G/G (*N* = 46), G/A (*N* = 46), and A/A (*N* = 12). No significant differences were observed among the three groups in any clinical characteristics. While preoperative cerebral infarctions tended to occur more frequently in the A/A group, the difference was not statistically significant, and ICH was rare with minimal differences among groups. The mean follow-up duration was 49.7 months, with the A/A group showing a slightly longer mean follow-up of 63.3 months. At the last follow-up, an mRS score of 0 was most common, accounting for 50% (*N* = 52), and when dichotomized, 96% (*N* = 100) had an mRS score ≤ 2.

Characterization of the CSF Proteome in MMD Patients

To delineate alterations in the CSF proteome associated with MMD, we analyzed 118 CSF samples from 14 HC and 104 MMD patients, including individuals with the G/G (*N* = 46), G/A (*N* = 46), and A/A (*N* = 12) genotypes (Fig. 1A). LC–MS/MS analysis was performed based on the label-free quantification of all the samples from HC and MMD patients. Employing our robust workflow without depletion of high-abundance proteins, we identified a total of 2463 proteins, with 2307 proteins quantified in at least one sample (Supplementary Table 1). On average, approximately 1200 proteins were quantified per CSF sample (Fig. 1B). A Venn diagram showed that 31 proteins were uniquely identified in HC and 278 in MMD (Fig. 1C), while extensive overlap was observed across the three genotypes (Fig. 1D). Compared with previous label-free CSF proteomic studies [37], our proteomic approach provided substantially deeper proteome coverage. Protein abundance in MMD CSF spanned approximately six orders of magnitude (Supplementary Fig. 1 A).

The $\log_2$-transformed intensity distribution of quantified proteins demonstrated high stability of our MS platform. To evaluate reproducibility, Pearson's correlation coefficient was calculated from five randomly selected samples per group (Supplementary Fig. 1B), averaging 0.75 for HC and 0.82 for MMD. Reproducibility remained high within genotype subgroups, with correlation coefficients ranging from 0.79–0.82 (G/G), 0.80–0.87 (G/A), and 0.80–0.88 (A/A) (Supplementary Fig. 1 C).

Unsupervised analysis of sample distribution via principal component analysis (PCA) revealed clear separation between HC and MMD along the first component that the first component (Fig. 1E), whereas MMD genotypes could not be distinguished by the first two principal components (Fig. 1F).

Table 1 Demographic characteristics of Moyamoya disease and hydrocephalus patients

	MMD (*N* = 104)	HC (*N* = 14)	*P*-value
Sex			1.000
Male	55 (53%)	7 (50%)	
Female	49 (47%)	7 (50%)	
Age (years)	8.1 ± 4.1	2.5 ± 4.1	< 0.001
Cause of HC			
Chiari malformation type 1		7 (50%)	
Chiari malformation type 2		1 (7%)	
Osteogenesis imperfecta		1 (7%)	
Dandy-Walker syndrome		1 (7%)	
Crouzon syndrome		1 (7%)	
Arachnoid cyst		1 (7%)	
Germinal matrix hemorrhage		2 (14%)	

MMD moyamoya disease, *HC* hydrocephalus

Comparison of the CSF Proteome Profiles Between HC and MMD Groups

Comparison of CSF proteome profiles between HC and MMD groups, irrespective of genotype, revealed a dramatic shift in the quantitative proteome composition. A total of 321 DEPs were identified, including 162 upregulated and 159 downregulated proteins in MMD (Student's *t*-test, FDR adjusted $P < 0.05$; Fig. 2A and Supplementary Table 2). Notably, previously reported MMD marker candidates such as albumin (ALB) and CRABP-1 [14, 38] were among the DEPs. Further stratification of MMD patients by genotype demonstrated no significant changes in CSF proteome composition in pairwise comparisons among G/G, G/A, and A/A groups, consistent with PCA findings (Supplementary Fig. 2).

To characterize the biological relevance of the altered proteins, pathway enrichment analysis via EnrichR was performed. Upregulated proteins in MMD were predominantly enriched, associated with TGF-β regulation of the extracellular matrix (ECM) and complement and coagulation

Table 2 Demographic and clinical characteristics of moyamoya disease patients overall and those with the RNF 213 p.P4810K genotype

Genotype	All ($N=104$)	G/G ($N=46$)	G/A ($N=46$)	A/A ($N=12$)	*P*-value
Sex					0.651
Male	55 (53%)	26 (57%)	22 (48%)	7 (58%)	
Female	49 (47%)	20 (43%)	24 (52%)	5 (42%)	
Age (years)	8.1 ± 4.1	8.0 ± 4.3	8.7 ± 3.3	6.8 ± 6.0	0.348
Bilaterality					0.928
Definite	89 (86%)	40 (87%)	39 (85%)	10 (83%)	
Probable	15 (14%)	6 (13%)	7 (15%)	2 (17%)	
Suzuki stage					0.385
1 ~ 3	78 (75%)	36 (78%)	35 (76%)	7 (58%)	
4 ~ 6	26 (25%)	10 (22%)	11 (24%)	5 (42%)	
Preoperative cerebral infarction					0.058
Yes	29 (28%)	12 (26%)	10 (22%)	7 (58%)	
No	75 (72%)	34 (74%)	36 (78%)	5 (42%)	
Preoperative ICH					1.000
Yes	3 (3%)	1 (2%)	2 (4%)	0 (0%)	
No	101(97%)	45 (98%)	44 (96%)	12 (100%)	
Operation side					0.106
Bilateral	82 (79%)	40 (87%)	32 (70%)	10 (83%)	
Unilateral	22 (21%)	6 (13%)	14 (30%)	2 (17%)	
mRS					0.189
0	52 (50%)	19 (41%)	26 (57%)	7 (58%)	
1	43 (41%)	25 (54%)	15 (33%)	3 (25%)	
2	5 (5%)	1 (2%)	2 (4%)	2 (17%)	
3	1 (1%)	0 (0%)	1 (2%)	0 (0%)	
4	1 (1%)	0 (0%)	1 (2%)	0 (0%)	
5	2 (2%)	1 (2%)	1 (2%)	0 (0%)	
mRS					0.767
0~2	100 (96%)	43 (94%)	45 (98%)	12 (100%)	
3~5	4 (4%)	3 (6%)	1 (2%)	0 (0%)	
Follow up duration (months)	49.7 ± 34.3	55.4 ± 32.9	40.4 ± 34.1	63.3 ± 34.2	0.036

ICH intracerebral hemorrhage, *mRS* modified Rankin scale, *RNF* ring finger protein

cascades, whereas downregulated proteins were enriched in lysosomal pathways (Fig. 2B, Supplementary Fig. 3 A). Integrated functional analyses using IPA identified 126 significantly enriched canonical pathways (Supplementary Table 3). PPI network mapping of these pathways further confirmed strong enrichment of ECM organization and complement and coagulation cascades in MMD CSF (Supplementary Fig. 3B), consistent with EnrichR results.

To identify a protein-based signature with diagnostic power, the top 10 DEPs were selected via feature selection algorithms, including ANOVA, infoGain, ReliefF, and fast correlation-based filter (FCBF). This approach yielded 19 high-ranking proteins, with three (VIM, SPARC, and SFRP1) consistently prioritized across all methods. Signal intensity analysis revealed that 8 of these proteins were significantly upregulated, while 11 were downregulated in MMD (Fig. 2D). Proteomic findings for the 8 upregulated proteins (ALB, BLVRA, F13A1, VIM, CNDP1, SLITRK1, OGN, and PKM) were validated via ELISA (Supplementary Fig. 4), confirming the increased expression of ALB and SLITRK1 in MMD patients, irrespective of genotype (Fig. 2E, Supplementary Fig. 5A and B). Subgroup analyses across the Overlap group (samples overlapping with the discovery cohort), Non-overlap group (independent validation samples not included in discovery), and Full validation cohort (all validation samples combined) demonstrated that SLITRK1 consistently showed significant differences between MMD and HC groups, confirming its robustness, whereas ALB reached significance only in the Non-overlap and Full cohorts, highlighting the importance of an independent validation cohort (Supplementary Fig. 5 C).

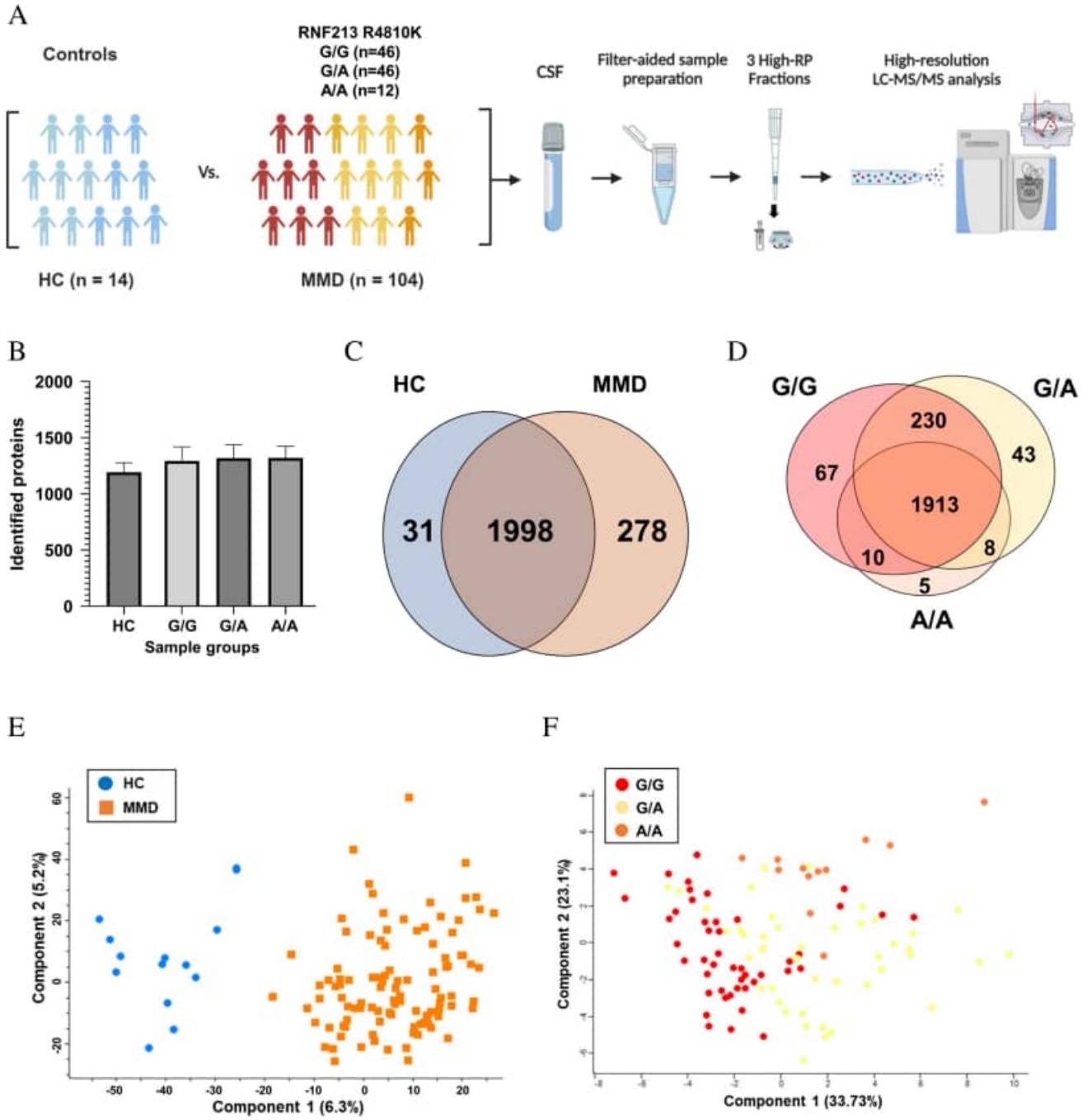

Fig. 1 Cerebrospinal fluid (CSF) proteome characterization of moyamoya disease (MMD). **A** Liquid chromatography with tandem mass spectrometry (LC−MS/MS)-based proteomic workflow for identifying the CSF proteome of MMD patients. **B** Number of proteins identified with a 1% false discovery rate (FDR) in each sample group. The error bars indicate the standard deviation (SD). **C** Overlap of quantified proteins between hydrocephalus (HC) and MMD groups. **D** Overlap of quantified proteins among the RNF213 p.P4810K genotypes. **E** Principal component analysis (PCA) of proteins in total CSF samples. HC patients are represented in blue, and MMD patients are represented in orange. **F** PCA of proteins in CSF samples from MMD patients with three genotypes. G/G, G/A, and A/A are represented in red, yellow, and orange, respectively

Stepwise logistic regression based on ALB and SLITRK1 was employed to identify a subset of proteins capable of distinguishing between MMD and HC groups. Leave-one-out cross-validation yielded mean areas under the receiver operating characteristic curve (AUROCs) of 0.966 and 0.926 for ALB and SLITRK1, respectively (Supplementary Fig. 6).

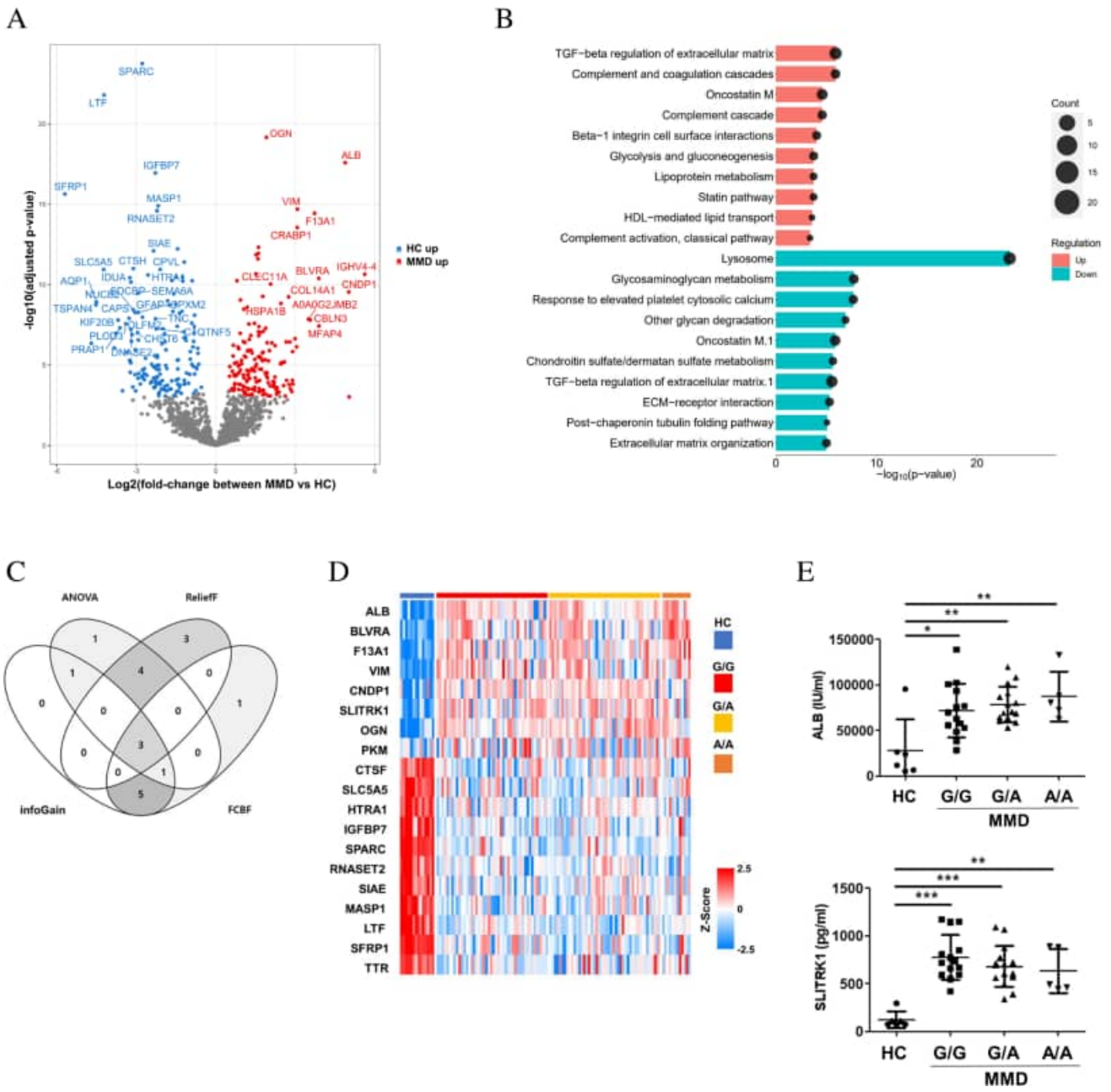

Fig. 2 Differences in the cerebrospinal fluid (CSF) proteome between hydrocephalus (HC) and moyamoya disease (MMD) patients. **A** Volcano plot showing fold-change values and statistical significance between HC and MMD patients, as determined by Student's *t*-test. Red indicates upregulated proteins, blue indicates downregulated proteins in MMD patients, and colored proteins are statistically significant (FDR adjusted $P < 0.05$). **B** Different pathways between CSF samples from HC and MMD patients. **C** Feature selection of proteins for classification. Feature selection was performed via ANOVA, ReliefF, infoGain, and fast correlation-based filter (FCBF) for differentially expressed proteins (DEPs). The top 10 candidates from each algorithm are shown, with proteins highly ranked across all algorithms displayed in overlapping circles. **D** Heatmap of selected proteins expressed in CSF samples from HC and MMD patients. **E** Validation of the levels of ALB and SLITRK1 via ELISA across HC and MMD subgroups (G/G, G/A, and A/A). Statistical significance was determined using one-way ANOVA followed by Tukey's post hoc test. $***P < 0.001$; $**P < 0.01$; $*P < 0.05$; and *P*-values from independent *t*-tests are shown

Clinical Factors Associated with the Proteomic Profiles of CSF Samples from MMD Patients

To evaluate associations between clinical factors and the CSF proteome in MMD, we performed WGCNA, an unsupervised approach that identifies groups of coregulated proteins and their links to clinical factors [28]. A signed weighted network was constructed using Pearson's correlation with a soft thresholding power of 8 to achieve a scale-free topology ($R^2 \geq 0.9$) (Supplementary Fig. 7). The resulting network comprised 8 protein modules, ranging from 19 to 756 proteins (Fig. 3 and Supplementary Table 4).

Module–trait correlations were examined for sex, age, Suzuki stage, cerebral infarction, ICH and mRS. Several modules, such as module eigengene (ME) yellow (109 proteins), MEblue (216 proteins), MEgreen (70 proteins), MEblack (60 proteins), MEred (67 proteins), MEbrown (212 proteins), and MEturquoise (756 proteins) were found to be correlated with at least one clinical factor tested (Spearman correlation ≥ 0.1 and nominal P-value ≤ 0.05) (Fig. 4A). Gene Ontology (GO) enrichment analysis revealed that sex-associated modules (MEyellow, MEblue, MEred, and MEturquoise) were enriched for immune response, fibrinolysis, metabolic process, and cell adhesion. Suzuki stage correlated with MEyellow (immune response), while cerebral infarction correlated with MEred (metabolic processes, inflammation, and vesicle-mediated transport). ICH was associated with MEblue and MEbrown (fibrinolysis and metabolic processes), and mRS score was linked to MEyellow and MEblack (immune response, cell morphology, and microtubule organization).

Cell-type enrichment analysis, based on reference RNA sequencing datasets for astrocytes, endothelial cells, microglia, neurons, and oligodendrocytes [33, 39], showed that MEblue and MEbrown-two closely relate endothelial cell-enriched modules-were associated with ICH. MEred, enriched in astrocyte and microglial markers, demonstrated strong positive correlations with cerebral infarction.

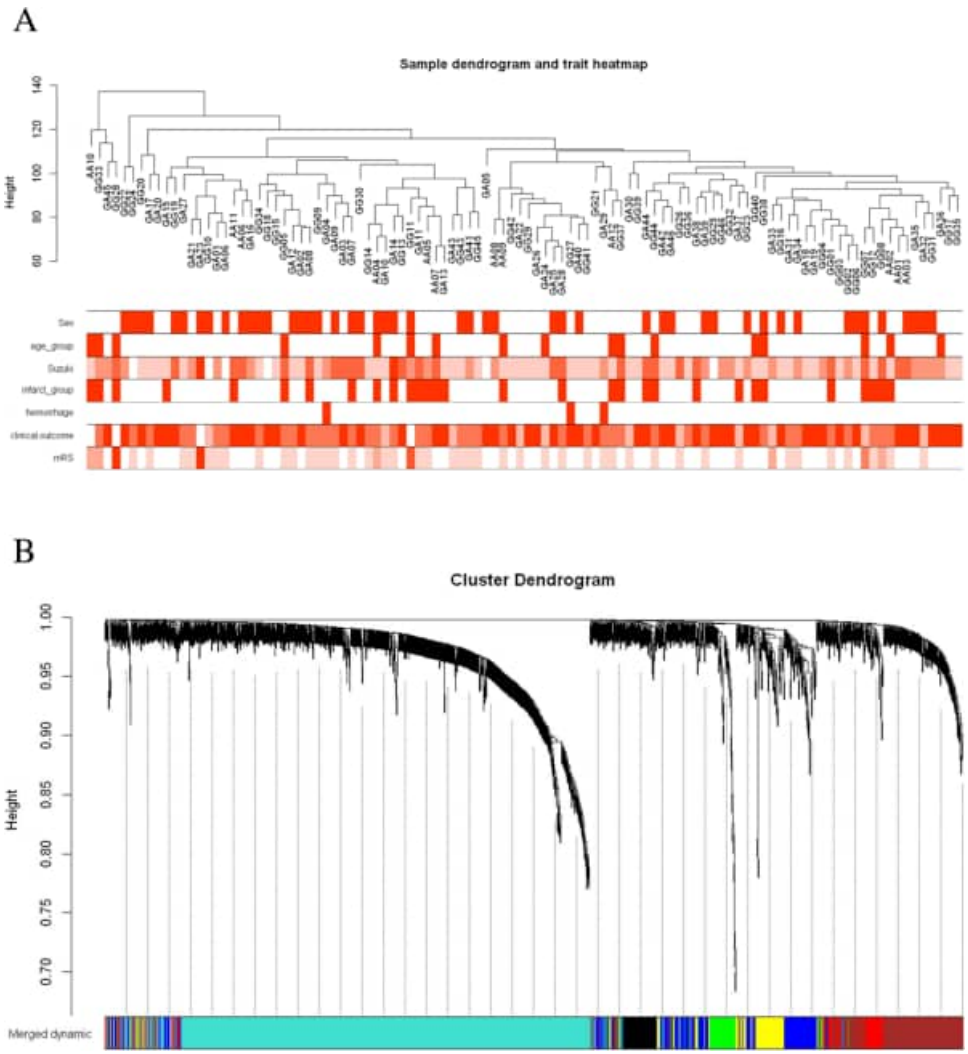

Fig. 3 Protein coexpression network construction. **A** Sample dendrogram and trait heatmap. **B** Cluster dendrograms of the proteins with the topological overlap measure dissimilarity matrix, with module colors assigned by the initial dynamic tree cut and the final merged dynamic, which are identical

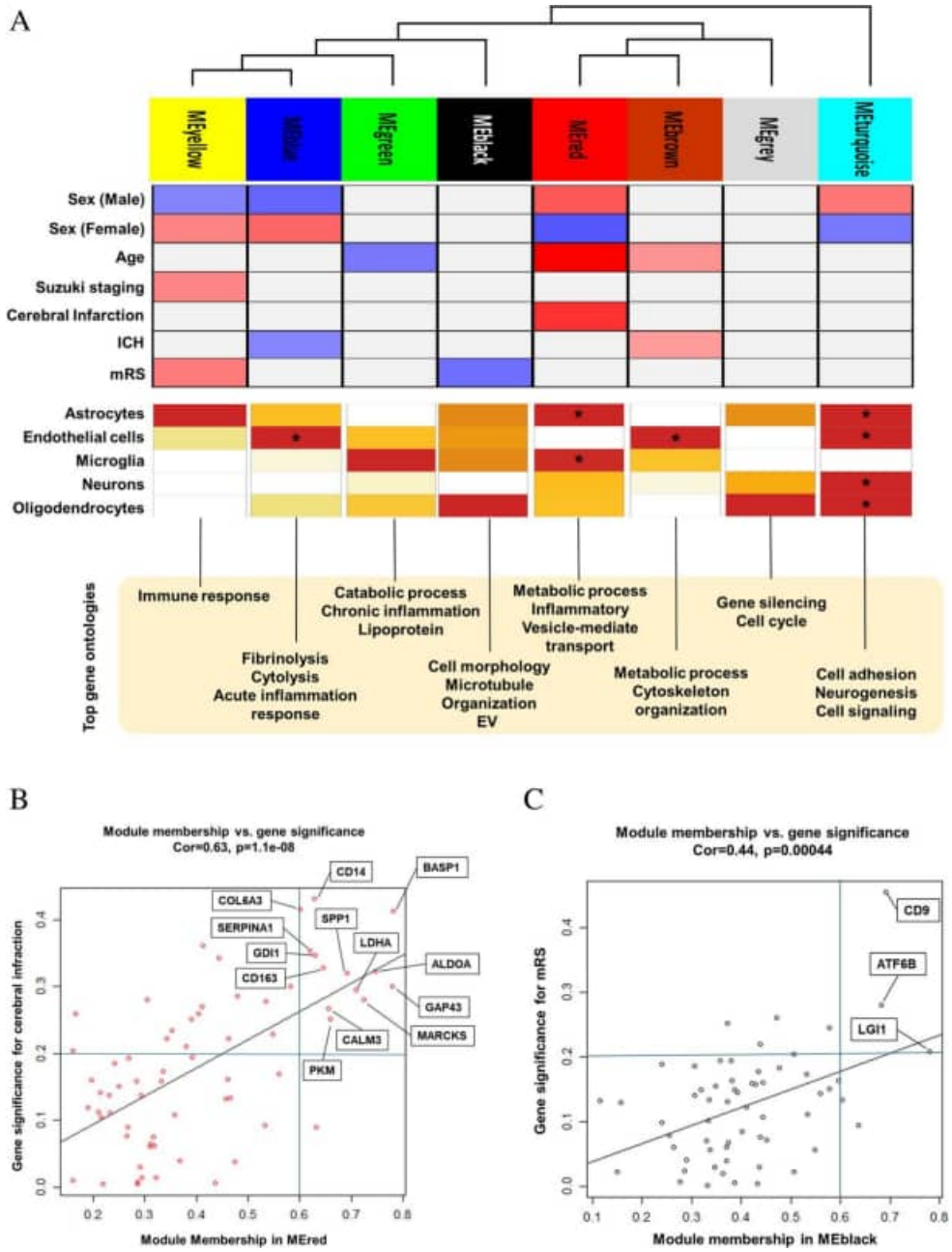

Fig. 4 Clinical factors associated with cerebrospinal fluid (CSF) proteomic profiles of patients with moyamoya disease (MMD). **A** Module assignment and cluster dendrogram. Highly interconnected genes were clustered, and eight modules were identified via hierarchical clustering tree analysis. Different colors represent different modules. The strengths of the positive (red) and negative (blue) correlations are illustrated in the two-color heatmap. Pearson correlation coefficients and *P*-values were calculated via the weighted gene coexpression network analysis package. The cell type of each module was assessed by module protein overlapping with cell-type-specific marker lists of astrocytes, endothelial cells, microglia, neurons, and oligodendrocytes. Gene ontology enrichment analysis of each module was performed via the DAVID bioinformatics tool, with statistical significance determined by Fisher's exact test. ICH: intracerebral hemorrhage. $*P < 0.05$. **B** Hub genes defined by module membership (MM) and gene significance (GS) in MEred. The MM is plotted on the *x*-axis, the GS is plotted on the *y*-axis, and each point represents an individual protein within each module. Thirteen hub proteins were identified according to an MM > 0.6 and a GS > 0.2 within MEred. **C** Hub genes defined by MM and GS in MEblack. Three hub genes were identified according to an MM > 0.6 and a GS > 0.2 within MEblack. **D** Protein−protein interaction (PPI) network depiction of proteins in MEred that are positively correlated with cerebral infarction. Nodes represent proteins (red), and edges (lines) indicate connections between the nodes. The grey nodes represent interacting partners connected to input proteins involved in MEred. Hub proteins are shown in yellow. **E** PPI network depiction of MEblack, which is negatively correlated with the mRS score. Nodes represent proteins (black), and edges (lines) indicate connections between nodes. Grey nodes are interacting partners connected to input proteins involved in MEblack. Hub proteins are shown in yellow

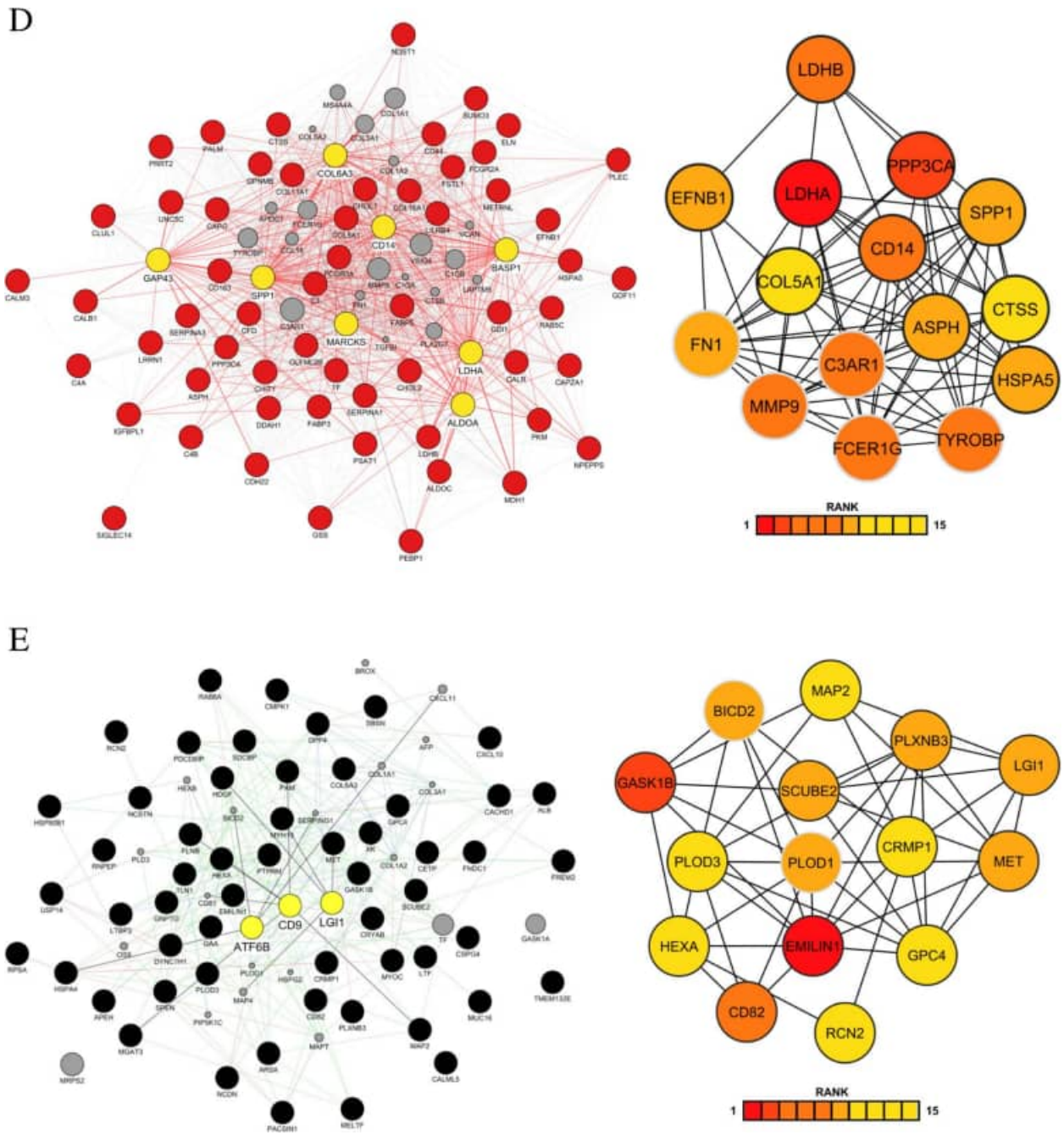

Fig. 4 (continued)

Identification of Hub Proteins That Predict Clinical Outcomes

Pairwise comparison of CSF proteome based on cerebral infarction status or clinical outcome (mRS) revealed distinct proteomic profiles between MMD patients with cerebral infarction or unfavorable clinical outcomes and those without cerebral infarction or with favorable clinical outcomes (Supplementary Fig. 8). To identify key proteins with prognosis, we focused on two protein modules (MEred and MEblack) that showed strong correlations with cerebral infarction and clinical outcome.

In MEred, a significant linear relationship between module membership and protein significance for cerebral infarction was observed (Fig. 4B). Thirteen hub proteins (|MM|> 0.2 and |GS|> 0.6) were identified: BASP1, GAP43, ALDOA, CD14, COL6A3, SPP1, MARCKS, LDHA, GDI1, CD163, SERPINA1, CALM3, and PKM. In MEblack, a

significant linear relationship between module membership and protein significance for the mRS was observed (Fig. 4C), and three hub proteins were identified: CD9, ATF6B, and LGI1. PPI network analysis revealed that several hub genes, such as BASP1, CD14, SPP1, COL6A3, ALDOA, LDHA, GAP43, and MARCK3, served as key nodes in MEred. Topological analysis further revealed that three hub proteins (LDHA, CD14, and SPP1) were among the top 15 bottleneck nodes (Fig. 4D). In MEblack, the PPI network revealed interconnections among the hub proteins (LGI1, CD9, and ATF6B). Notably, only LGI1 was among the top 15 bottleneck nodes (Fig. 4E). Interestingly, EMILIN1 and GASK1B were identified as the top bottleneck proteins despite not being identified as hub proteins.

Additionally, we analyzed whether the aforementioned markers were differently expressed in patients. Expression analyses confirmed that BASP1 and LDHA were upregulated in patients with cerebral infarction (BASP1: $P < 0.0001$, LDHA: $P < 0.0049$) (Supplementary Fig. 9). Pearson correlation analysis of the CSF proteome against mRS scores (Supplementary Fig. 10) revealed that higher CD9 expression correlated with better clinical outcomes (Fig. 5A). Notably, CD9 expression was significantly lower in MMD patients compared with HC patients (Fig. 5B).

Discussion

Lack of RNF213 Genotype-Dependent Changes in CSF Proteome in MMD

RNF213 is a well-known susceptibility gene for MMD and has been reported to influence the clinical course and disease severity in previous studies [34–36]. However, in our cohort, pairwise comparisons among the three RNF213 genotypes revealed no significant shift in the quantitative CSF proteome composition. Several studies have suggested that RNF213 alone may be insufficient to fully explain the pathophysiological mechanisms of MMD, implying the requirement of a "second hit" [40, 41]. This concept has also been proposed as a potential reason for the failure to recapitulate MMD phenotypes in animal models. Our findings are consistent with these observations, supporting the notion that additional genetic or environmental factors may be necessary to drive disease manifestation.

Activated Biological Processes in MMD Patients: TGF-β Regulation of the ECM and Complement and Coagulation Cascades

TGF-β is a growth factor that regulates cell growth, differentiation, and gene expression in the ECM, as well as angiogenesis [42]. Overexpression of TGF-β is associated with phenotype changes in vascular smooth muscle cells, resulting in increased ECM production and elastin synthase accumulation [43]. This phenotypic switching from a differentiated/contractile to a dedifferentiated/synthetic state has been implicated in several pathological processes in MMD, including myointimal hyperplasia, vessel wall degeneration, matrix degradation, and distal ICA narrowing [44, 45]. Additionally, TGF-β can promote angiogenesis in collateral vessels such as moyamoya vessels [43, 46]. In line with this, Zhang et al. [47] reported that overexpression of cytoskeletal proteins FLNA and ZYX induces pathological vascular remodeling via AKT/GSK-3β/β-catenin signaling. Since cytoskeletal reorganization is closely linked to ECM dynamics and endothelial cell motility, these findings suggest that

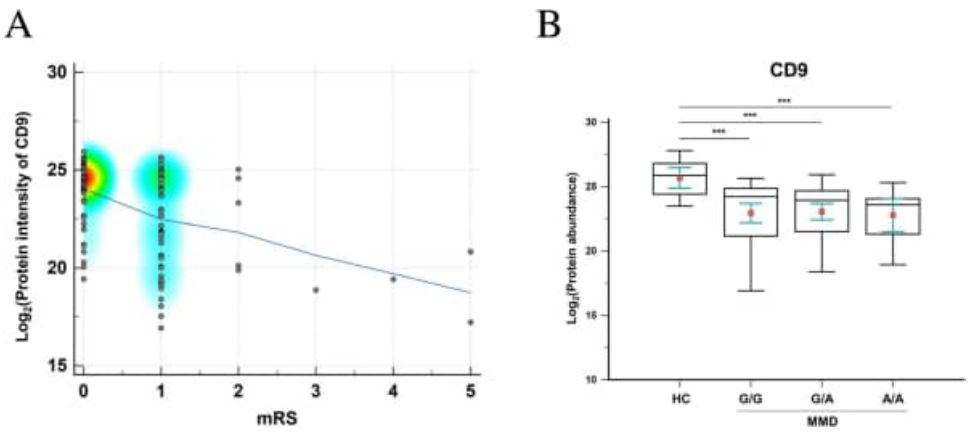

Fig. 5 Correlation analysis between the cerebrospinal fluid (CSF) proteome and clinical outcome in moyamoya disease (MMD) patients. **A** Correlation plot between CD9 and modified Rankin Scale (mRS) score. **B** Protein abundance of CD9 among the hydrocephalus (HC), G/G, G/A, and A/A genotypes in CSF MMD samples. Statistical significance was determined by Student's *t*-test. Boxplots show the median (central line), upper and lower quartiles (box limits), and 1.53 interquartile range (whiskers) ***$P < 0.001$

TGF-β–mediated ECM remodeling and cytoskeletal alterations may synergistically contribute to abnormal angiogenesis and intimal hyperplasia in MMD.

The complement and coagulation cascades are essential biological processes involved in blood clotting and immune responses [48]. Dysregulated activation of these pathways can provoke vascular inflammation and immune-mediated injury, contributing to cardiovascular diseases, cerebral ischemia, and other pathological neurologic disorders [49, 50]. In MMD, upregulation of complement C1 inhibitor has been associated to progressive stenosis of the distal ICA [51]. Moreover, elevated thrombosis-related markers, such as D-dimer, have been suggested as potential prognostic markers for disease recurrence and adverse neurological outcomes, particularly in pediatric arterial ischemic stroke [52].

A Novel Diagnostic Biomarker of MMD: Albumin and SLITRK1

Albumin is not synthesized in the CNS. The CSF/serum albumin ratio serves as a measure of blood−brain barrier (BBB) integrity. Elevated CSF albumin level may reflect brain inflammation or hemorrhage [53] and has been proposed as a potential marker for disease progression in Parkinson's disease [54]. However, this elevation is generally considered as a secondary consequence of BBB disruption rather than a primary pathogenic factor, and its direct relevance to the pathogenesis of MMD remains unclear.

SLITRK1 belongs to a family of integral membrane proteins characterized by two N-terminal leucine-rich repeat domains and a C-terminal region homologous to TRK neurotrophin receptors [55]. It is known to regulate neurite outgrowth and has been implicated in Tourette syndrome [56]. In our study, SLITRK1 was proposed for the first time as a potential biomarker associated with MMD. Previous work using in vitro neurovascular models demonstrated that vascular endothelial cells can significantly promote neurite elongation, indicating that endothelial cells influence neuronal morphology not only through structural support but also via cell–cell interactions mediated by secreted factors [57–59]. Given the characteristic endothelial proliferation observed in MMD, this observation suggests a possible mechanistic link. However, establishing a direct association between SLITRK1 and vasculopathy remains theoretically challenging. Further studies are warranted to clarify the role of SLITRK1 and MMD pathogenesis.

BASP1 and LDHA Are Cerebral Infarction-Related Markers, and CD9 and EMILIN1 Are Clinical Outcome-Related Markers in MMD Patients

Preoperative cerebral infarction was significantly correlated with MEred, whereas the mRS score was significantly associated with MEblack. Within MEred, BASP1 demonstrated the most significant linear relationship between module membership and protein significance, and LDHA emerged as the most crucial hub gene in the PPI network, suggesting that its upregulation may be linked to cerebral infarction. In MEblack, CD9 showed the most significant linear relationship between module membership and protein significance, while EMILIN1 was identified as the key hub gene in the PPI network, indicating that its upregulation may be associated with favorable clinical outcomes.

BASP1 (brain abundant, membrane-attached signal protein 1) is known for its role in synapse formation during brain development [60]. Recent studies have linked BASP1 overexpression to coronary heart disease, implicating it in endothelial cell dysfunction [61]. In our cohort, CSF samples were obtained after the onset of cerebral infarction, making it unclear whether elevated BASP1 levels reflect neuronal injury secondary to infarction or whether BASP1 contributes to endothelial dysfunction that predisposes to infarction. Further studies are required to clarify this cause–effect relationship.

LDHA, lactate dehydrogenase A, is a critical metabolic enzyme in the 2-hydroxy acid oxidoreductases family that plays a central role in anaerobic metabolism. Under hypoxic conditions, LDHA overexpression shifts ATP production from oxidative phosphorylation to aerobic glycolysis [62]. LDHA is expressed in both brain tissue and smooth muscle. If elevated LDHA levels in the CSF originate from brain tissue, they may represent a secondary response to hypoxia following cerebral infarction. Conversely, previous reports have suggested that increased glycolysis in vascular smooth muscle cells promotes proliferation and migration, leading to an atherogenic phenotype, and that LDHA may serve as a therapeutic target to prevent vessel lumen narrowing [63]. Taken together, these findings raise the possibility that LDHA upregulation may contribute to the development of cerebral infarction. Further research is required to identify the cellular source of LDHA in CSF.

CD9, a membrane protein expressed in various cell types including immune cells, is involved in multiple biological processes such as cell adhesion, motility, growth, and signal transduction [64]. Brosseau et al. [64] reviewed experimental and clinical evidence identifying CD9 as a regulator of inflammatory pathways, underscoring its broad roles in vascular and immune regulation. Mannion et al. [65], using an in vitro wound repair assay, demonstrated that CD9 is directly involved in angiogenesis by promoting endothelial cell migration. Furthermore, Kamisasanuki et al. [66] demonstrated that suppression of CD9 in activated endothelial cells in a CD9 knockdown mouse model resulted in stimulus-independent antiangiogenic effects, confirming the role of CD9 as a key modulator of angiogenesis. In the present

study, CD9 expression was decreased in patients with MMD, and lower expression levels were associated with poorer functional status. These findings are consistent with previous reports linking CD9 to vascular remodeling and neural cell motility, suggesting that decreased CD9 may contribute to the cerebrovascular pathology of MMD. Taken together with follow-up data, our results support a potential relationship between CD9 expression and clinical outcomes, warranting further investigation into whether CD9 levels influence neovascularization after revascularization surgery.

EMILIN1 (elastin microfibril interface–located protein 1) is associated with elastin in the ECM of arteries, the lymph vasculature, and other tissues [67]. It contributes to vessel wall integrity and elasticity by organizing elastin deposits and inhibits TGF-β activation by blocking proteolytic processing of the latency-associated peptide/active TGF-β complex. EMILIN1 expression in the middle cerebral artery has been reported to influence vessel autoregulation, with deficiency linked to impaired responses to changes in blood pressure [68]. In MMD patients, EMILIN1 may affect postoperative angiogenesis or regulate cerebral blood flow autoregulation, potentially impacting prognosis. However, the usefulness of EMILIN1, along with CD9, in assessing patient prognosis, should be validated in prospective studies involving future patient cohorts.

Comparison with Recent CSF-Based Studies in MMD

Earlier studies identified elevated levels of CRABP-1 [38] and haptoglobin [17] in MMD CSF as potential contributors to pathogenesis, while more recent reports have proposed Angiopoietin-2 [69] and Cadherin-18 [70] as prognostic biomarkers. In our pediatric cohort, CRABP-1 was detected among the DEPs, though it was not among the most highly ranked. Similarly, haptoglobin showed an upregulation but did not reach statistical significance. Notably, Angiopoietin-2, previously linked to poor prognosis, demonstrated a marginally significant upregulation in the unfavorable outcome group. Cadherin-18 was also detected in our dataset, but due to a high rate of missing values, it was excluded from further statistical analyses. These differences from earlier findings, primarily derived from adult patient populations, may reflect age-dependent variations in CSF proteomic profiles.

Limitations

First, the characteristics between HC and MMD groups were not matched, and their epidemiological profiles differed, making alignment challenging. Collecting CSF from healthy children with similar demographic features is not only impractical but also ethically unfeasible. To include the most appropriate control group, we excluded tumor-associated HC patients and focused on patients requiring CSF diversion surgery for pure HC. This reflects the most appropriate clinical scenario in our setting. Additionally, as anesthesia and surgical procedures can induce substantial proteomic changes, HC patients who undergo surgery may serve as better controls than normal healthy individuals. Second, the disease etiologies underlying our HC patients are diverse, which may result in subtle baseline differences in the CSF proteome and thus increase intra-group variance compared to the homogeneity expected in a healthy control group. We acknowledge this clinical heterogeneity within the HC group as a limitation and recognize that this variability may have influenced our findings and should be considered when interpreting our results. Third, the markers identified in our study as associated with the onset or prognosis of MMD (e.g., cerebral infarction, ICH) exhibited correlation rather than causal relationships. Therefore, the underlying pathophysiology remains unclear, and further studies are necessary to elucidate causal relationships. Fourth, this study did not include a validation cohort to assess reproducibility or evaluate external validity. Future studies are warranted to confirm these findings and extend their applicability. Finally, although an independent validation set was included in the ELISA analysis, a partial overlap with the discovery proteomics cohort may have introduced verification bias. This potential bias should be considered when interpreting the results. Additionally, the small number of HC samples, particularly in the overlapping group ($N=2$), limited the statistical power for subgroup analyses. Further studies using larger and fully independent cohorts will be necessary to confirm the generalizability and robustness of our findings.

Conclusions

In this study, comprehensive proteomic screening of CSF from a large MMD cohort provided novel insights into the CSF proteome of MMD patients. We identified SLITRK1 as a potential novel biomarker that may be associated to MMD pathogenesis. Additionally, BASP1 and LDHA were identified as markers linked to preoperative cerebral infarction, while CD9 and EMILIN1 were associated with clinical outcome. These markers hold promises as candidate biomarkers for the diagnosis and potential therapeutic targeting of MMD.

Supplementary Information The online version contains supplementary material available at https://doi.org/10.1007/s12975-025-01384-8.

Author Contribution Dohyn Han and Seung-Ki Kim designed the study. Seung Ah Choi, Ji Hoon Phi, and Seung-Ki Kim collected the

data. Youngbo Shim, Seung Ah Choi, and Kisoon Dan statistically analyzed the data and drafted the manuscript. Eun Jung Koh, Saehim Ha, Ji Hoon Phi, Joo Whan Kim, Dohyun Han, and Seung-Ki Kim revised the manuscript. All authors read and approved the final version for publication. All the authors significantly contributed to the content of the manuscript.

Funding This work was supported by a National Research Foundation of Korea (NRF) grant funded by the Korean government (MSIT, 2019R1A2C209009911), the SNUH Research Fund by the Seoul National University Hospital (No. 26-20200030), and the SNUH Kunhee Lee Child Cancer and Rare Disease Project, Republic of Korea (Grant Number: 23C-027-0100).

Data Availability The mass spectrometry proteomics data have been deposited to the ProteomeXchange Consortium via the PRIDE partner repository with the dataset identifier PXD059285.

Declarations

Ethics Approval and Consent to Participate This study was performed in line with the principles of the Declaration of Helsinki. This study was approved by the Institutional Review Board of our institute (No. 2011-191-1178) and informed consent was waived due to the retrospective study design.

Competing Interests The authors declare no competing interests.

References

1. Takeuchi K. Hypoplasia of bilateral internal carotid arteries. No To Shinkei. 1957;9:37–43.
2. Suzuki J, Takaku A. Cerebrovascular, "moyamoya" disease. Disease showing abnormal net-like vessels in base of brain. Arch Neurol. 1969;20:288–99.
3. Takagi Y, Kikuta K, Nozaki K, Hashimoto N. Histological features of middle cerebral arteries from patients treated for Moyamoya disease. Neurol Med Chir (Tokyo). 2007;47:1–4.
4. Derdeyn CPM, Pollak LM, Scott RMM, Smith ERM. Moyamoya disease and moyamoya syndrome. The New England Journal of Medicine. 2009;361:97-; author reply 8.
5. Piao J, Wu W, Yang Z, Yu J. Research progress of Moyamoya disease in children. Int J Med Sci. 2015;12:566–75.
6. Zheng J, Yu LB, Dai KF, Zhang Y, Wang R, Zhang D. Clinical features, surgical treatment, and long-term outcome of a multicenter cohort of pediatric Moyamoya. Front Neurol. 2019;10:14.
7. Kim T, Oh CW, Bang JS, Kim JE, Cho WS. Moyamoya disease: treatment and outcomes. J Stroke. 2016;18:21–30.
8. Acker G, Fekonja L, Vajkoczy P. Surgical management of Moyamoya disease. Stroke. 2018;49:476–82.
9. Kuroda S, Nanba R, Ishikawa T, Houkin K, Kamiyama H, Iwasaki Y. [Clinical manifestations of infantile moyamoya disease]. No Shinkei Geka. 2003;31:1073–8.
10. Liu W, Morito D, Takashima S, Mineharu Y, Kobayashi H, Hitomi T, et al. Identification of RNF213 as a susceptibility gene for moyamoya disease and its possible role in vascular development. PLoS ONE. 2011;6:e22542.
11. Kamada F, Aoki Y, Narisawa A, Abe Y, Komatsuzaki S, Kikuchi A, et al. A genome-wide association study identifies RNF213 as the first Moyamoya disease gene. J Hum Genet. 2011;56:34–40.
12. Shoemaker LD, Clark MJ, Patwardhan A, Chandratillake G, Garcia S, Chen R, et al. Disease Variant Landscape of a Large Multiethnic Population of Moyamoya Patients by Exome Sequencing. G3 (Bethesda). 2015;6:41–9.
13. Dorschel KB, Wanebo JE. Genetic and proteomic contributions to the pathophysiology of Moyamoya angiopathy and related vascular diseases. Appl Clin Genet. 2021;14:145–71.
14. Kim SK, Yoo JI, Cho BK, Hong SJ, Kim YK, Moon JA, et al. Elevation of CRABP-I in the cerebrospinal fluid of patients with Moyamoya disease. Stroke. 2003;34:2835–41.
15. Rüggeberg S, Horn P, Li X, Vajkoczy P, Franz T. Detection of a gamma-carboxy-glutamate as novel post-translational modification of human transthyretin. Protein Pept Lett. 2008;15:43–6.
16. Maruwaka M, Yoshikawa K, Okamoto S, Araki Y, Sumitomo M, Kawamura A, et al. Biomarker research for moyamoya disease in cerebrospinal fluid using surface-enhanced laser desorption/ionization time-of-flight mass spectrometry. J Stroke Cerebrovasc Dis. 2015;24:104–11.
17. Kashiwazaki D, Uchino H, Kuroda S. Downregulation of apolipoprotein-E and apolipoprotein-J in Moyamoya disease-a proteome analysis of cerebrospinal fluid. J Stroke Cerebrovasc Dis. 2017;26:2981–7.
18. Hervé D, Ibos-Augé N, Calvière L, Rogan C, Labeyrie MA, Guichard JP, et al. Predictors of clinical or cerebral lesion progression in adult moyamoya angiopathy. Neurology. 2019;93:e388–97.
19. Perez-Riverol Y, Bai J, Bandla C, García-Seisdedos D, Hewapathirana S, Kamatchinathan S, et al. The PRIDE database resources in 2022: a hub for mass spectrometry-based proteomics evidences. Nucleic Acids Res. 2022;50(D1):D543–52.
20. Han D, Moon S, Kim Y, Kim J, Jin J, Kim Y. In-depth proteomic analysis of mouse microglia using a combination of FASP and StageTip-based, high pH, reversed-phase fractionation. Proteomics. 2013;13:2984–8.
21. Tyanova S, Temu T, Cox J. The maxquant computational platform for mass spectrometry-based shotgun proteomics. Nat Protoc. 2016;11:2301–19.
22. Cox J, Hein MY, Luber CA, Paron I, Nagaraj N, Mann M. Accurate proteome-wide label-free quantification by delayed normalization and maximal peptide ratio extraction, termed MaxLFQ. Mol Cell Proteomics. 2014;13:2513–26.
23. Jang HN, Moon SJ, Jung KC, Kim SW, Kim H, Han D, et al. Mass spectrometry-based proteomic discovery of prognostic biomarkers in adrenal cortical carcinoma. Cancers (Basel). 2021;13.
24. Cox J, Neuhauser N, Michalski A, Scheltema RA, Olsen JV, Mann M. Andromeda: a peptide search engine integrated into the MaxQuant environment. J Proteome Res. 2011;10:1794–805.
25. Tyanova S, Temu T, Sinitcyn P, Carlson A, Hein MY, Geiger T, et al. The perseus computational platform for comprehensive analysis of (prote)omics data. Nat Methods. 2016;13:731–40.
26. Kramer A, Green J, Pollard J Jr, Tugendreich S. Causal analysis approaches in Ingenuity Pathway Analysis. Bioinformatics. 2014;30:523–30.
27. Szklarczyk D, Gable AL, Nastou KC, Lyon D, Kirsch R, Pyysalo S, et al. The STRING database in 2021: customizable protein-protein networks, and functional characterization of user-uploaded gene/measurement sets. Nucleic Acids Res. 2021;49(D1):D605–12.
28. Langfelder P, Horvath S. WGCNA: an R package for weighted correlation network analysis. BMC Bioinformatics. 2008;9:559.
29. von Mering C, Huynen M, Jaeggi D, Schmidt S, Bork P, Snel B. STRING: a database of predicted functional associations between proteins. Nucleic Acids Res. 2003;31:258–61.
30. Szklarczyk D, Gable AL, Lyon D, Junge A, Wyder S, Huerta-Cepas J, et al. STRING v11: protein-protein association networks with increased coverage, supporting functional discovery in genome-wide experimental datasets. Nucleic Acids Res. 2019;47:D607–13.

31. Shannon P, Markiel A, Ozier O, Baliga NS, Wang JT, Ramage D, et al. Cytoscape: a software environment for integrated models of biomolecular interaction networks. Genome Res. 2003;13:2498–504.
32. Guo L, Lin W, Zhang Y, Li W, Wang J. BEST: a web server for brain expression spatio-temporal pattern analysis. BMC Bioinformatics. 2019;20:632.
33. Zhang Y, Sloan SA, Clarke LE, Caneda C, Plaza CA, Blumenthal PD, et al. Purification and characterization of progenitor and mature human astrocytes reveals transcriptional and functional differences with mouse. Neuron. 2016;89:37–53.
34. Kim EH, Yum MS, Ra YS, Park JB, Ahn JS, Kim GH, et al. Importance of RNF213 polymorphism on clinical features and long-term outcome in moyamoya disease. J Neurosurg. 2016;124:1221–7.
35. Miyatake S, Miyake N, Touho H, Nishimura-Tadaki A, Kondo Y, Okada I, et al. Homozygous c.14576G>A variant of RNF213 predicts early-onset and severe form of moyamoya disease. Neurology. 2012;78:803–10.
36. Miyatake S, Touho H, Miyake N, Ohba C, Doi H, Saitsu H, et al. Sibling cases of moyamoya disease having homozygous and heterozygous c.14576G>A variant in RNF213 showed varying clinical course and severity. J Hum Genet. 2012;57:804–6.
37. Vervuurt M, Schrader JM, de Kort AM, Kersten I, Wessels H, Klijn CJM, et al. Cerebrospinal fluid shotgun proteomics identifies distinct proteomic patterns in cerebral amyloid angiopathy rodent models and human patients. Acta Neuropathol Commun. 2024;12:6.
38. Jeon JS, Ahn JH, Moon YJ, Cho WS, Son YJ, Kim SK, et al. Expression of cellular retinoic acid-binding protein-I (CRABP-I) in the cerebrospinal fluid of adult onset moyamoya disease and its association with clinical presentation and postoperative haemodynamic change. J Neurol Neurosurg Psychiatry. 2014;85:726–31.
39. Seyfried NT, Dammer EB, Swarup V, Nandakumar D, Duong DM, Yin L, et al. A multi-network approach identifies protein-specific co-expression in asymptomatic and symptomatic Alzheimer's disease. Cell Syst. 2017;4:60-72.e4.
40. Letchuman V, Ampie L, Mastorakos P, Raper DMS, Kellogg RT, Park MS. Experimental animal models for the study of moyamoya disease. Neurosurg Focus. 2021;51:E4.
41. Moteki Y, Onda H, Kasuya H, Yoneyama T, Okada Y, Hirota K, et al. Systematic validation of RNF213 coding variants in Japanese patients with Moyamoya disease. J Am Heart Assoc. 2015. https://doi.org/10.1161/JAHA.115.001862.
42. Bedini G, Blecharz KG, Nava S, Vajkoczy P, Alessandri G, Ranieri M, et al. Vasculogenic and angiogenic pathways in Moyamoya disease. Curr Med Chem. 2016;23:315–45.
43. Yamamoto M, Aoyagi M, Tajima S, Wachi H, Fukai N, Matsushima Y, et al. Increase in elastin gene expression and protein synthesis in arterial smooth muscle cells derived from patients with Moyamoya disease. Stroke. 1997;28:1733–8.
44. Milewicz DM, Kwartler CS, Papke CL, Regalado ES, Cao J, Reid AJ. Genetic variants promoting smooth muscle cell proliferation can result in diffuse and diverse vascular diseases: evidence for a hyperplastic vasculomyopathy. Genet Med. 2010;12:196–203.
45. Yu X, Li Z. Micrornas regulate vascular smooth muscle cell functions in atherosclerosis (review). Int J Mol Med. 2014;34:923–33.
46. Massagué J. TGFβ signalling in context. Nat Rev Mol Cell Biol. 2012;13:616–30.
47. He S, Zhang J, Liu Z, Wang Y, Hao X, Wang X, et al. Upregulated cytoskeletal proteins promote pathological angiogenesis in Moyamoya disease. Stroke. 2023;54:3153–64.
48. Amara U, Rittirsch D, Flierl M, Bruckner U, Klos A, Gebhard F, et al. Interaction between the coagulation and complement system. Adv Exp Med Biol. 2008;632:71–9.
49. Oksjoki R, Kovanen PT, Meri S, Pentikainen MO. Function and regulation of the complement system in cardiovascular diseases. Front Biosci. 2007;12:4696–708.
50. Ziabska K, Ziemka-Nalecz M, Pawelec P, Sypecka J, Zalewska T. Aberrant complement system activation in neurological disorders. Int J Mol Sci. 2021. https://doi.org/10.3390/ijms22094675.
51. Koh EJ, Kim HN, Ma TZ, Choi HY, Kwak YG. Comparative analysis of serum proteomes of moyamoya disease and normal controls. J Korean Neurosurg Soc. 2010;48:8–13.
52. Bernard TJ, Fenton LZ, Apkon SD, Boada R, Wilkening GN, Wilkinson CC, et al. Biomarkers of hypercoagulability and inflammation in childhood-onset arterial ischemic stroke. J Pediatr. 2010;156:651–6.
53. Reiber H, Peter JB. Cerebrospinal fluid analysis: disease-related data patterns and evaluation programs. J Neurol Sci. 2001;184:101–22.
54. Pisani V, Stefani A, Pierantozzi M, Natoli S, Stanzione P, Franciotta D, et al. Increased blood-cerebrospinal fluid transfer of albumin in advanced Parkinson's disease. J Neuroinflammation. 2012;9:188.
55. Beaubien F, Raja R, Kennedy TE, Fournier AE, Cloutier JF. Slitrk1 is localized to excitatory synapses and promotes their development. Sci Rep. 2016;6:27343.
56. Aruga J, Mikoshiba K. Identification and characterization of Slitrk, a novel neuronal transmembrane protein family controlling neurite outgrowth. Mol Cell Neurosci. 2003;24:117–29.
57. Aksan B, Mauceri D. Beyond vessels: unraveling the impact of VEGFs on neuronal functions and structure. J Biomed Sci. 2025;32:33.
58. Asaba T, Osaki T, Murayama K, Hamano S, Kageyama T, Fukuda J. Effects of vascular endothelial cells on the neurite outgrowth of nerve cells. J Biosci Bioeng. 2025;140:168–73.
59. Sumimoto S, Muramatsu R, Fujii S, Yamashita T. Vascular endothelial cells promote cortical neurite outgrowth via an integrin β3-dependent mechanism. Biochem Biophys Res Commun. 2014;450:593–7.
60. Manganas LN, Durá I, Osenberg S, Semerci F, Tosun M, Mishra R, et al. BASP1 labels neural stem cells in the neurogenic niches of mammalian brain. Sci Rep. 2021;11:5546.
61. Sun F, Liu J, Wang Y, Yang H, Song D, Fu H, et al. BASP1 promotes high glucose-induced endothelial apoptosis in diabetes via activation of EGFR signaling. J Diabetes Investig. 2023;14:535–47.
62. Burgner JW 2nd, Ray WJ Jr. On the origin of the lactate dehydrogenase induced rate effect. Biochemistry. 1984;23:3636–48.
63. Kim JH, Bae KH, Byun JK, Lee S, Kim JG, Lee IK, et al. Lactate dehydrogenase-A is indispensable for vascular smooth muscle cell proliferation and migration. Biochem Biophys Res Commun. 2017;492:41–7.
64. Brosseau C, Colas L, Magnan A, Brouard S. CD9 tetraspanin: a new pathway for the regulation of inflammation? Front Immunol. 2018;9:2316.
65. Klein-Soyer C, Azorsa DO, Cazenave JP, Lanza F. Cd9 participates in endothelial cell migration during in vitro wound repair. Arterioscler Thromb Vasc Biol. 2000;20:360–9.
66. Kamisasanuki T, Tokushige S, Terasaki H, Khai NC, Wang Y, Sakamoto T, et al. Targeting CD9 produces stimulus-independent antiangiogenic effects predominantly in activated endothelial cells

during angiogenesis: a novel antiangiogenic therapy. Biochem Biophys Res Commun. 2011;413:128–35.
67. Randell A, Daneshtalab N. Elastin microfibril interface-located protein 1, transforming growth factor beta, and implications on cardiovascular complications. J Am Soc Hypertens. 2017;11:437–48.
68. Daneshtalab N, Smeda JS. Alterations in the modulation of cerebrovascular tone and blood flow by nitric oxide synthases in SHRsp with stroke. Cardiovasc Res. 2010;86:160–8.
69. Gorla G, Potenza A, Carrozzini T, Pollaci G, Acerbi F, Vetrano IG, et al. Angiopoietin-2 associates with poor prognosis in Moyamoya angiopathy. Ann Clin Transl Neurol. 2024;11:1590–603.
70. Guo D, Dong Y, Li H, Li H, Yang B. Proteomics and digital subtraction angiography approaches reveal CDH18 as a potential target for therapy of moyamoya disease. Biol Direct. 2024;19:76.